EFFICIENT COMPUTATION OF COORDINATE-FREE MODELS OF FLAME FRONTS

BENJAMIN F. AKERS AND DAVID M. AMBROSE

Abstract. We present an efficient, accurate computational method for a coordinate-free model of flame front propagation of Frankel and Sivashinsky. This model allows for overturned flames fronts, in contrast to weakly nonlinear models such as the Kuramoto-Sivashinksy equation. The numerical procedure adapts the method of Hou, Lowengrub and Shelley, derived for vortex sheets, to this model. The result is a non-stiff, highly accurate solver which can handle fully nonlinear, overturned interfaces, with similar computational expense as methods for weakly nonlinear models. We apply this solver both to simulate overturned flame fronts and to compare the accuracy of Kuramoto-Sivashisky and coordinate-free models in the appropriate limit.

1. Introduction

We study a model for one-dimensional flame fronts moving in two spatial dimensions developed by Frankel and Sivashinsky [7]. Such models specify the velocity by which the front moves, in terms of intrinsic geometric information, namely curvature and arclength. While these models allow for general geometries, flame fronts are more commonly studied with weakly nonlinear models such as the Kuramoto-Sivashinsky equation which places constraints on the geometry, such as that the height of the front is a single-valued function of horizontal position. Recently, Goto et al. directly simulated a model without assuming weak nonlinearity [9]. The numerical method in [9] used finite difference discretization in space and fourth-order Runge-Kutta for timestepping, and thus is subject to a classic explicit timestep restriction. In this contribution, we demonstrate that fully nonlinear, coordinate-free models may be efficiently simulated. In particular, we introduce a non-stiff method for the initial value problem which is pseudospectral with respect to spatial variables and which uses implicit-explicit timestepping, avoiding the time step restriction present in [9].

The method is based on the work of Hou, Lowengrub, and Shelley (HLS) for interfacial fluid flows with surface tension [10], [11]. The HLS method is based on evolving geometric quantities naturally related to the curvature; specifically, these were the tangent angle the interface forms with the horizontal, and the arclength element. Since curvature and arclength are

fundamental to the models of [7], we find that the HLS formulation applies. This formulation, when combined with IMEX time-stepping, yields a non-stiff method for the propagation of flame fronts.

Coordinate-free models specify the normal velocity of the flame front; denoting the normal velocity by U and the curvature of the front by κ, one model presented in [7] is

$$-U = 1+(\alpha-1)\kappa+\left(1+\frac{\alpha^2}{2}\right)\kappa^2+\left(2\alpha+5\alpha^2-\frac{\alpha^3}{3}\right)\kappa^3+\alpha^2(\alpha+3)\kappa_{ss}. \tag{1}$$

With α near unity, and neglecting small terms, another model is derived from (1) in [7]:

$$-U = 1+(\alpha-1)\kappa+4\kappa_{ss}. \tag{2}$$

The term κ_{ss} is the second derivative of curvature with respect to arclength. The parameter α allows the lower-order term κ to be destabilizing at low wavenumbers/long wavelengths if $\alpha > 1$. For interfaces which are functions of the spatial coordinate, with $\alpha \approx 1$ with small, slowly-varying data, these models are approximated by the Kuramoto-Sivashinky equation

$$y_t + (\alpha-1)y_{xx} + 4y_{xxxx} + \frac{1}{2}(y_x)^2 = 0. \tag{3}$$

The paper [7] that we have mentioned several times already introduced the coordinate-free models that we study for the case of two spatial dimensions. Other related work includes the extension to three spatial dimensions [8] and the introduction of temperature effects [6]. Numerical simulations conducted in these papers are fully explicit and use finite differences. Of course fully explicit methods for fourth-order equations have severe stiffness constraints; as mentioned above, we introduce here a pseudo-spectral method using semi-implicit timestepping. Our method is therefore highly accurate without significant timestep constraints. We develop and validate the numerical method in Section 2.

Along with the development of the coordinate-free models in [7], the Kuramoto-Sivashinksy equation is derived as a weakly nonlinear model starting from these coordinate-free models. One may naturally ask, then, as to the validity of the approximations involved in such a derivation. In Section 3, we implement our numerical method to demonstrate the asymptotic validity of the Kuramoto-Sivashinsky equation as an approximation to the coordinate-free models in the appropriate regime. The second author, along with Hadadifard and Wright, has also demonstrated this validity fully rigorously [3]. A related work is [5], in which solutions of two different weakly nonlinear models related to coordinate-free models of flame fronts are shown to remain close over time; one of these weakly nonlinear models is the Kuramoto-Sivashinsky equation. It is explicitly stated in [5] that the weakly nonlinear models are to be preferred because of the ease of numerical simulation; we demonstrate here that by our method, the full coordinate-free model may be simulated at essentially the same cost.

There is another advantage of using the fully nonlinear coordinate-free models which we simulate, and that is that there is no assumption that the interface is a graph with respect to one variable; weakly nonlinear models such as the Kuramoto-Sivashinsky equation inherently have this restriction to graphs. Our final simulation shown in Section 3 is of an interface with multi-valued height, which is thus beyond the reach of the weakly nonlinear models.

2. Problem formulation

Let a curve $(x(\sigma,t), y(\sigma,t))$ be evolving in $\mathbb{R}^2$; then we define the arclength element s_σ and the tangent angle the curve forms with the horizontal, θ, as

$$s_\sigma = \sqrt{x_\sigma^2 + y_\sigma^2}, \qquad \theta = \tan^{-1}(y_\sigma/x_\sigma).$$

In terms of these quantities, the curvature of the interface is

$$\kappa = \frac{\theta_\sigma}{s_\sigma}. \tag{4}$$

We denote a frame of normal and tangent vectors at each point of the curve as

$$\hat{\mathbf{n}} = \frac{(-y_\sigma, x_\sigma)}{s_\sigma}, \qquad \hat{\mathbf{t}} = \frac{(x_\sigma, y_\sigma)}{s_\sigma}.$$

We let U denote the normal velocity of the interface and V denote the tangential velocity,

$$(x,y)_t = U\hat{\mathbf{n}} + V\hat{\mathbf{t}}.$$

In terms of U and V, we may infer evolution equations for s_σ and θ, which are

$$s_{\sigma t} = V_\sigma - \theta_\sigma U, \qquad \theta_t = \frac{U_\sigma + V\theta_\sigma}{s_\sigma}. \tag{5}$$

We take x and y to be spatially periodic in the following sense:

$$x(\sigma + 2\pi, t) = M + x(\sigma, t), \qquad y(\sigma + 2\pi, t) = y(\sigma, t),$$

for a fixed $M > 0$. Then θ is also 2π-periodic: $\theta(\sigma + 2\pi, t) = \theta(\sigma, t)$, for all σ and t.

While U is specified by (1) or (2), the tangential velocity, V, may be chosen to enforce a preferred parameterization of the front. We take a normalized arclength parameterization. Letting $L(t)$ be the length of one period of the curve, we require s_σ to satisfy $s_\sigma = L/2\pi$. We see then, using the $s_{\sigma t}$ equation in (5) together with the requirement that s_σ be independent of σ, that

$$L_t = -\int_0^{2\pi} \theta_\sigma U \, d\sigma. \tag{6}$$

With this normalized arclength parameterization, the formula (4) becomes

$$\kappa = \frac{2\pi\theta_\sigma}{L}. \tag{7}$$

We may then write the second derivative of curvature with respect to arclength as

$$\kappa_{ss} = \frac{\kappa_{\sigma\sigma}}{s_\sigma^2} = \frac{\theta_{\sigma\sigma\sigma}}{s_\sigma^3} = \frac{(2\pi)^3\theta_{\sigma\sigma\sigma}}{L^3}. \tag{8}$$

We introduce the projection $\mathbb{P}$, which removes the mean of a periodic function,

$$\mathbb{P}f = f - \frac{1}{2\pi}\int_0^{2\pi} f(\sigma)\, d\sigma.$$

The normalized arclength parameterization requires $s_{\sigma t} = L_t/2\pi$, but we also have the equation for $s_{\sigma t}$ in (5). This gives us the tangential velocity

$$V = \partial_\sigma^{-1}\mathbb{P}(\theta_\sigma U),$$

In the numerical section that follows, we evolve (6) and

$$\theta_t = \frac{2\pi}{L}\left(U_\sigma + \theta_\sigma\partial_\sigma^{-1}\mathbb{P}(\theta_\sigma U)\right) \tag{9}$$

with U defined as either the fully nonlinear (1) or the weakly nonlinear (2). We compare the asymptotics of evolution small amplitude, slowly varying data in these two models to the same data in Kuramoto-Sivashinsky (3).

3. Numerical method

3.1. **Specification of the method.** In this section we discuss the numerical method and simulations of the coupled system of (6) and (9) (using either closure (1) or (2), coupled with curvature formulas (7) and (8)). This system is numerically approximated using Fourier collocation for spatial derivatives (as well as for the integral in equation (6)). To approximate the time evolution of the discretized system we follow HLS, and implement the 4^{th} order IMEX scheme of Ascher, Ruuth & Wetton [4]. This time stepper is designed for an ODE of the form $u_t = f(u) + g(u)$ (typically one chooses $f(u)$ to be linear and $g(u)$ the nonlinearity). It updates as

$$\begin{aligned}\frac{1}{\Delta t}\left(\frac{25}{12}u^{n+1} - 4u^n + 3u^{n-1} - \frac{4}{3}u^{n-2} + \frac{1}{4}u^{n-3}\right) = \\ f(u^{n+1}) + 4g(u^n) - 6g(u^{n-1}) + 4g(u^{n-2}) - g(u^{n-3}).\end{aligned} \tag{10}$$

This scheme is not self starting, and one needs to use another scheme for the first three steps. We compare three potential initializations: direct implementation of a fourth-order Runge-Kutta (RK4), an RK4 scheme supplemented with integrating factors (as in [12, 13]), and a third order Richardson-extrapolation of the following first order IMEX scheme:

$$\frac{u^{n+1} - u^n}{\Delta t} = f(u^{n+1}) + g(u^n). \tag{11}$$

All three initializations result in a fourth-order accurate scheme, whose stability restriction is dictated by that of (10) in the limit of small time step. In practice, the stability restrictions of the initialization manifest when one

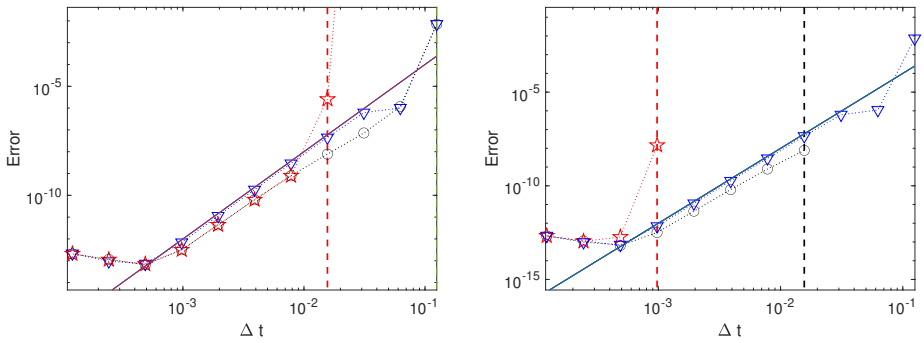

FIGURE 1. *The convergence rate of the IMEX4 method* (10) *is depicted. The markers denote three choices of initialization methods. Direct RK4 initialization is marked with stars; RK4 with integrating factors is marked with circles; a Richardson extrapolated IMEX1 is marked with triangles. A solid line at* 4^{th} *order accuracy also depicted for comparison purposes. The left panel has* $N_\sigma = 16$ *spatial points; the right panel has* $N_\sigma = 32$ *spatial points. The stiffness of this system manifests as a maximum time step (marked with dashed vertical lines) at which the schemes with the RK4 initialization give finite output (the schemes give infinite output to the right of this dashed line). We do not observe any time step restriction for the Richardson-extrapolated IMEX1 initialization.*

is far outside their stability region, causing the numerical trajectories to overflow their storage type in the early steps. We present this phenomena in Figure 1 and Figure 2. The linear stability region of RK4 is well known, and we observe that integrating factors do little to ameliorate this stability restriction in this problem. Linear stability analysis on the scheme (11), applied to the test problem $f = u_{\sigma\sigma\sigma\sigma}$ and $g = au_\sigma$ gives a scheme which is stable for $\Delta t \leq O(\frac{1}{a^2})$ (independent of the number of points in space). This is precisely the behavior we observe numerically when using the Richardson-extrapolation of equation (11) as an initialization method for (10); the resulting scheme's stability properties appear to be independent of spatial resolution.

3.2. **Stability of the method.** In Figure 1, we evaluate the convergence and stability of each initialization method. In the left panel of Figure 1, we fix the number of points in space as $N_\sigma = 16$ and observe that each initialization gives the promised fourth-order accuracy. In the right panel of this figure, we see that increasing to $N_\sigma = 32$ there is a maximum time step for which one can use the RK4 based initializations (marked with vertical dashed lines in this panel). The Richardson-extrapolated IMEX1 initialization had no observed time step restriction when creating these plots. All

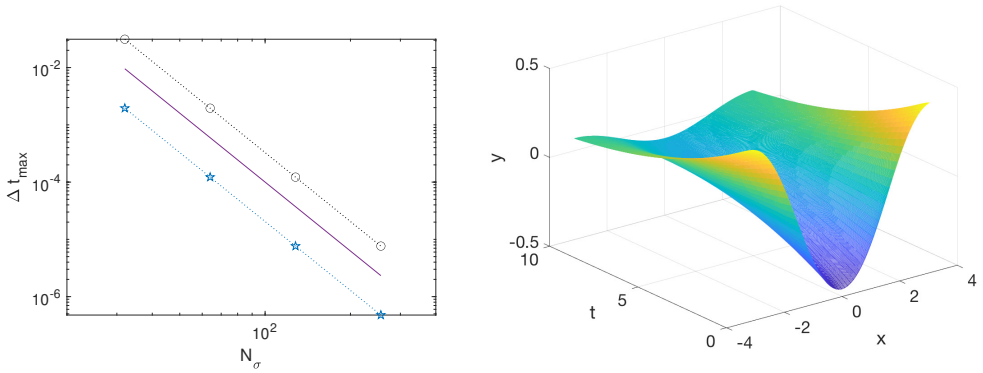

FIGURE 2. *The stability of the different initializations of the IMEX4 method is depicted. The left panel shows the observed time step restriction as a function of total spatial points (N_σ) As in Figure 1, the stars correspond to direct RK4 initialization and the circles are the integrating factor RK4 initialization. We do not observe any time step restriction when initializing with the Richardson-extrapolated IMEX1 scheme (thus there are no triangles marking its maximum time step in the left panel). We have run simulations with the number of spatial points, N_σ, up to $2^{16} = 65536$ and observed stable computations with $\Delta t = 0.1$ with this initialization for long times; this simulation is the the right panel. The same initial data was used for the simulations used to create the left panel, but with $t < 1/4$.*

three methods are ultimately fourth order and stable for sufficiently small time step.

In Figure 2, we estimate the CFL condition for these schemes by running the scheme at a sampling of N_σ and tracking the largest time step for which the scheme is stable. For the purposes of this simulation we call the scheme unstable if it has solution with $\|\theta\|_\infty > 10$ before $t = 1/4$; the resolved solution we tested on had $\|\theta\|_\infty < \pi/2$. We observe that both RK4 based initializations have a CFL condition which scales like $\Delta t \leq C(\Delta\sigma)^4$ (the solid line in the right panel). The Richardson-extrapolated IMEX1 initialization had no observable time step restriction; successful simulations were conducted with the scheme with $N_\sigma = 2^{16} = 65536$ and $\Delta t = 0.1$, see the right panel of Figure 2.

4. Results

4.1. **Asymptotic comparison of the models.** As an application of the numerical method, we compare the evolution of initial data

$$y(x) = \epsilon \sin(\sqrt{\epsilon} x), \qquad \alpha = 1 + \epsilon, \tag{12}$$

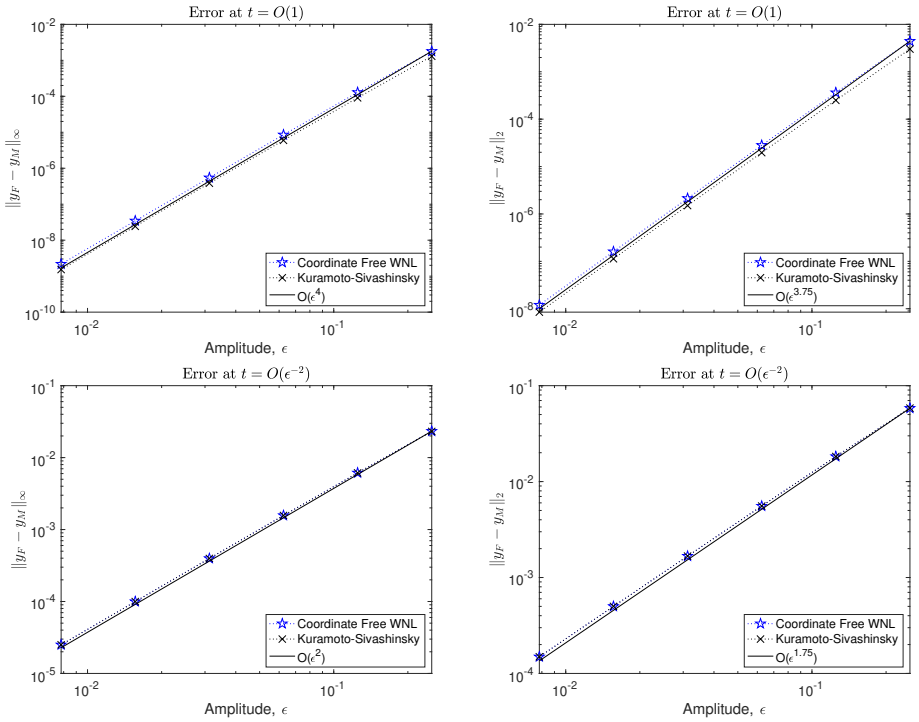

FIGURE 3. *The difference between the evolutions of the approximate models, Kuramoto-Sivashinksy* (3) *and the coordinate-free system with weakly nonlinear closure* (2)*, and the full coordinate-free model, where the normal velocity closure is* (1) *with initial data* (12)*. In the top row we compare solutions at fixed time; the bottom row the time is scaled like* $O(\epsilon^{-2})$*.*

in the Kuramoto-Sivashinsky equation, as well as the coordinate-free models of Frankel and Sivashinsky which use the normal velocities given in (1) and (2). To initialize the coordinate-free models, we construct the tangent angle and curve length using

$$\theta = \tan^{-1}(y_x), \qquad L = \int \sqrt{1 + y_x^2}\, dx.$$

As the weakly-nonlinear coordinate-free model, using (2), and the Kuramoto-Sivashinksy equation are approximations of the fully nonlinear coordinate-free model, using (1), we consider the fully nonlinear model as the truth and compare the other two models against it. The difference between the evolutions of this initial data (12) in the three model equations appear in Figure 3, in which the weakly nonlinear models are denoted y_M and the fully nonlinear model is denoted as y_F.

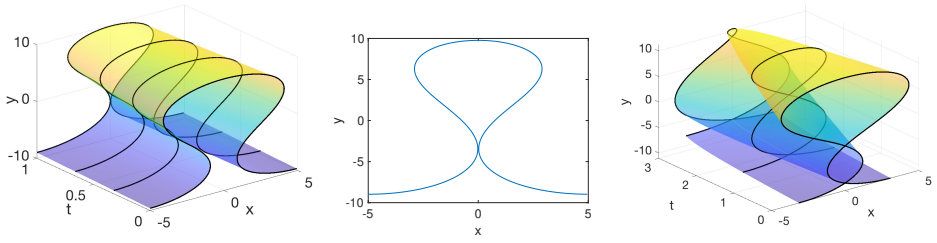

FIGURE 4. *The evolution of overturned initial data* (13) *with* $A = -11/17\pi, L \approx 48.7, M = 10$ *in the left (time evolution) and center panels (a profile near intersection at* $t = 2$*). The evolution of an example of self-intersecting initial data, with* $A = -7\pi/10, L \approx 56.6, M = 2\pi$ *is in the right panel.*

The derivation of the Kuramoto-Sivashinsky equation from coordinate-free models in [7] considers data scaled as in (12) and keeps term which are size $O(\epsilon^3)$ or smaller. The natural expectation would be for the errors created in this approximation to be asymptotically small compared to $O(\epsilon^3)$ for an $O(1)$ time interval. We observe infinity norm based error for a fixed time interval which scale as $O(\epsilon^4)$. The asymptotics of the infinity norm and the two-norm of the difference $y_F - y_M$ at both fixed and asymptotically long times are reported in the four panels of Figure 3. These rates match those in [3], suggesting that their rigorous bound is sharp in its asymptotic.

The coordinate-free solver discussed here has the same asymptotic cost as the Kuramoto-Sivashinksy equation (all of the equations can be evolved in $O(N_\sigma \log N_\sigma)$ flops per time step). The coordinate-free models have the advantage of being able to evolve initial data for which the interface displacement is not a function of the horizontal coordinate, but rather a general parameterized curve. In Figure 4 we present such simulations. For the simulations in Figure 4 we use initial data

$$\theta(\sigma) = A\sin(\sigma), \qquad \alpha = 0.1. \tag{13}$$

For fixed θ, the curve length, L, and spatial period, M, are related as

$$M = L\left(\frac{1}{2\pi}\int_0^{2\pi} \cos(\theta)\, d\sigma\right),$$

or

$$L = M\left(\frac{1}{2\pi}\int \cos(\theta)\, d\sigma\right)^{-1}.$$

We chose to initialize the spatial period, using the latter formula to initialize L.

4.2. **Evolution of an overturned interface.** The coordinate-free formulation allows for evolution of overturned interfaces, certainly an advantage as this allows for a larger simulation space. It also allows for the evolution of self-intersecting interfaces. These latter interfaces are non-physical, but

they do not create a singularity in the parametrically described equation (unlike in some other coordinate-free models like vortex sheets [1, 2]). An example of the evolution of a multiply self-intersecting interface is in the right panel of Figure 4.

Acknowledgments

The first author acknowledges support by Air Force Office of Scientific Research (AFOSR) though the Computational Mathematics Program. The second author gratefully acknowledges support from the National Science Foundation through grant DMS-1907684. The authors also thank J. Douglas Wright for helpful conversations.

References

[1] B.F. Akers, D.M. Ambrose, K. Pond, and J.D. Wright. Overturned internal capillary–gravity waves. *European Journal of Mechanics-B/Fluids*, 57:143–151, 2016.

[2] B.F. Akers, D.M. Ambrose, and J.D. Wright. Gravity perturbed crapper waves. *Proceedings of the Royal Society A: Mathematical, Physical and Engineering Sciences*, 470(2161):20130526, 2014.

[3] D.M. Ambrose, F. Hadadifard, and J.D. Wright. Well-posedness and asymptotics of a coordinate-free model of flame fronts. Preprint.

[4] U.M. Ascher, S.J. Ruuth, and B.T.R. Wetton. Implicit-explicit methods for time-dependent partial differential equations. *SIAM J. Num. Anal.*, 32(3):797–823, 1995.

[5] C.-M. Brauner, M.L. Frankel, J. Hulshof, A. Lunardi, and G.I. Sivashinsky. On the κ-θ model of cellular flames: existence in the large and asymptotics. *Discrete Contin. Dyn. Syst. Ser. S*, 1(1):27–39, 2008.

[6] M.L. Frankel, P.V. Gordon, and G.I. Sivashinsky. On disintegration of near-limit cellular flames. *Phys. Lett. A*, 310(5-6):389–392, 2003.

[7] M.L. Frankel and G.I. Sivashinsky. On the nonlinear thermal diffusive theory of curved flames. *J. Physique*, 48:25–28, 1987.

[8] M.L. Frankel and G.I. Sivashinsky. On the equation of a curved flame front. *Phys. D*, 30(1-2):28–42, 1988.

[9] M. Goto, K. Kuwana, and S. Yazaki. A simple and fast numerical method for solving flame/smoldering evolution equations. *JSIAM Letters*, 10:49–52, 2018.

[10] T.Y. Hou, J.S. Lowengrub, and M.J. Shelley. Removing the stiffness from interfacial flows with surface tension. *J. Comput. Phys.*, 114(2):312–338, 1994.

[11] T.Y. Hou, J.S. Lowengrub, and M.J. Shelley. The long-time motion of vortex sheets with surface tension. *Phys. Fluids*, 9(7):1933–1954, 1997.

[12] A.-K. Kassam and L.N Trefethen. Fourth-order time-stepping for stiff PDEs. *SIAM Journal on Scientific Computing*, 26(4):1214–1233, 2005.

[13] P.A. Milewski and E.G. Tabak. A pseudospectral procedure for the solution of nonlinear wave equations with examples from free-surface flows. *SIAM J. Sci. Comp.*, 21(3):1102–1114, 1999.

Department of Mathematics and Statistics, Air Force Institute of Technology, WPAFB, OH 45433 USA

Email address: benjamin.akers@afit.edu

Drexel University, Department of Mathematics, Philadelphia, PA 19104 USA

Email address: dma68@drexel.edu